SCIEPublish

Article

Modulation of the MEP Pathway for Overproduction of 13-R-manoyl Oxide in Cyanobacteria

Lawrence Chuk Sutardja [1], Nadia Dodge [2], Sandra Lambert Walby [1], Nicholas Jeffrey Butler [1], Thiyagarajan Gnanasekaran [3], Birger Lindberg Møller [4] and Poul Erik Jensen [2,*]

[1] Section for Molecular Plant Biology, Department of Plant and Environmental Sciences, University of Copenhagen, Blegdamsvej 3B, DK-2200 Copenhagen, Denmark; lsutardja@gmail.com (L.C.S.); sandra33@live.dk (S.L.W.); nicholash@sundew.bio (N.J.B.)

[2] Department of Food Science, University of Copenhagen, Rolighedsvej 26, DK-1958 Frederiksberg, Denmark; nadia.dodge@food.ku.dk (N.D.)

[3] Novo Nordisk Foundation Center for Basic Metabolic Research, University of Copenhagen, Blegdamsvej 3B, DK-2200 Copenhagen, Denmark; thiyagarajan.gnanasekaran@sund.ku.dk (T.G.)

[4] Plant Biochemistry Laboratory, Department of Plant and Environmental Sciences, University of Copenhagen, Blegdamsvej 3B, DK-2200 Copenhagen, Denmark; blm@plen.ku.dk (B.L.M.)

* Corresponding author. E-mail: peje@food.ku.dk (P.E.J.)

Received: 23 February 2024; Accepted: 21 March 2024; Available online: 22 March 2024

ABSTRACT: The cyanobacterium *Synechocystis* sp. PCC 6803 has gained scientific interest for its potential to use solar energy and atmospheric CO_2 for the production of high-value chemicals like pharmaceuticals, flavors, and fragrances. Forskolin is a diterpenoid found in the root cork of the plant *Plectranthus barbatus* and its biosynthetic pathway is initiated by two terpene synthases that convert geranylgeranyl diphosphate (GGDP) into the precursor 13-R-manoyl oxide (13-R-MO). Using the cyanobacterium *Synechocystis* sp. PCC 6803 as host, we expressed the two terpene synthases resulting in the synthesis of 0.83 mg/L 13-R-MO. Three different geranylgeranyl diphosphate synthases (GGDPSs) were selected for screening; a prokaryotic (*Synechococcus* sp. JA-3-3Ab (*Sj*)), a yeast (*Saccharomyces cerevisiae* (*Sc*)), and a plant (*P. barbatus* (*Pb*)) derived GGDPS. Strains containing the prokaryotic *Sj*- or the yeast *Sc*GGDPS consistently yielded more 13-R-MO than the base strain. By overexpression of 1-Deoxy-D-xylulose-5-phosphate synthase (DXS) positioned at the entry of the 2-C-methyl-d-erythritol 4-phosphate pathway (MEP) together with the prokaryotic *Sj*GGDPS, the 13-R-MO titer was increased 11-fold to reach 9.7 mg/L by boosting the synthesis of GGDP, the direct substrate for the diterpenoid synthases. We further show that application of a *n*-dodecane overlay to remove 13-R-MO from the culture medium provided a 2–3 fold increase of the 13-R-MO in a separate cultivation system.

Keywords: Diterpenoids, *Plectranthus barbatus*, *Synechocystis* sp. PCC 6803, GGDP synthase, Dodecane overlay, Light-driven production

1. Introduction

Cyanobacteria's ability to use solar radiation to fix atmospheric CO_2 provides the opportunity for engineering sustainable production of chemicals while simultaneously benefiting from their simple nutrient requirements and innate ability to occupy niches unsuitable for the production of food [1–3].

Terpenoids are the largest class of natural products and can be found in all living organisms [4,5]. Their structural and functional diversity affords many of the compounds with economic significance in the fragrance, cosmetics, food ingredients, and pharmaceutical industries. Much of our current production of terpenoids relies on traditional chemical synthesis or extraction and isolation from plant material [6]. Extraction from plants is often based on the use of organic solvents, proving wasteful with low yields of the desired terpenoid from significant amounts of plant biomass. The extraction of diterpenoids such as forskolin, ginkgolides, and triptonide, which are exclusively synthesized in the roots of their host plants, necessitates the excavation and harvesting of root materials [7–10]. However, this process invariably

https://doi.org/10.35534/sbe.2024.10005

destroys the plants, imposing additional adverse ecological costs such as soil erosion. Furthermore, each harvest demands the cultivation of a new generation of plants, leading to an increased demand for arable land.

Biosynthesis of terpenoids is dependent on complex modular processes. In cyanobacteria, the C5 isoprene building blocks are derived from the 2-C-methyl-d-erythritol 4-phosphate pathway (MEP pathway) [11]. The linear carbon skeletons of terpenoids are derived from the condensation of C5 isopentenyl diphosphate (IDP) and dimethylallyl diphosphate (DMADP). The length of the terpenoid is dependent on the number of C5 building blocks used as starting material for terpene synthases that catalyzes the production of monoterpenoids (C10), sesquiterpenoids (C15), and diterpenoids (C20). In the case of diterpenoids, diterpene synthases (diTPSs) catalyze the formation of multicyclic backbones, while functionalization of the cyclic structures is catalyzed by ER-bound cytochrome P450s (P450s) resulting in stereospecific and regioselective oxygenations [9,10,12–14].

In prokaryotes, the MEP pathway is the only pathway present for the production of terpenoid precursors. Cyanobacteria already produce terpenoids that are crucial for their photosynthetic machinery. These include the phytol tail of chlorophylls, carotenoids, tocopherols, and phylloquinones [11,15] Thus, cyanobacteria have an inherent potential as heterologous hosts for the production and storage of additional terpenoids [16].

A common strategy to improve terpenoid production is to increase the endogenous supply of precursor metabolites [17]. Overexpressing rate-limiting enzymes to enhance precursor supply is one commonly used strategy. The first committed step in the MEP pathway is the condensation of pyruvate and glyceraldehyde-3-phosphate (GAP) to yield 1-deoxy-D-xylulose-5-phosphate (DXP) catalyzed by 1-Deoxy-D-xylulose-5-phosphate synthase (DXS) [18]. DXS is the rate-limiting enzyme to control flux through the MEP pathway [19], and overexpression of DXS has led to increased titers of terpenes and terpenoids (reviewed in [20]). Likewise, the enzyme GGDP synthase (GGPDS) which condenses three molecules of IDP and one molecule of DMADP to form geranylgeranyl diphosphate (GGDP, C20), is the entry point leading to the biosynthesis of diterpenoids as well as carotenoids and the phytol tail of chlorophylls. Geranylgeranyl diphosphate synthase (GGDPS) is thus considered a key metabolic engineering target and accumulation of GGDP requires an uninhibited flux towards GGDP and usually a strong "metabolic pull" strategy is used by overexpressing GGDP synthase [21,22].

In this study, we focus on the initial steps of the biosynthetic pathway leading to the diterpenoid forskolin. Forskolin is naturally produced and present in the root cork of the plant *Plectranthus barbatus*. The initial steps in the forskolin pathway involves two terpene synthases (*Pb*TPS2 and *Pb*TPS3) [8]. A previous report showed that expression of *Pb*TPS2 and *Pb*TPS3 in *Synechocystis* resulted in the formation of 13-R-manoyl oxide (13-R-MO), a precursor in the forskolin pathway [23]. Here we report successful engineering by increasing carbon flux towards the endogenous metabolite GGDP which resulted in an 11-fold increase in production of 13-R-MO in comparison to the *Synechocystis* strain only expressing the two terpene synthases. We also demonstrate that removal of 13-R-MO from the culture medium using a dodecane overlay can potentially triple production, albeit in a different cultivation system.

2. Materials and Methods

2.1. Strains and Media

All cloning was performed using *E. coli* NEB 10-β carrying either pDF-trc [24] or pSL2387 (kind gift from Prof. Himadri Pakrasi) grown in standard LB media supplemented with 50 µg/mL spectinomycin or kanamycin. Conjugation was performed using *E. coli* strain HB101 carrying the helper plasmid pRL443 supplemented with 100 µg/mL carbenicillin in standard LB media. Wild type *Synechocystis PCC. 6803* and resulting strains were grown on solid BGH5 media or in liquid BGH11 media (BG5 or BG11 supplemented with 1.5 or 4.75 g/L HEPES, respectively) [25].

2.2. Culturing Conditions

2.2.1. Starter Cultures

Starter cultures were grown from freezer stocks on plates at 30 °C at approximately 50 µE irradiation using fluorescent lights. Liquid cultures were supplemented by flushing with 3% CO_2 (*v*/*v*).

2.2.2. Photobioreactor Cultures

Growth curves were performed on Multi Cultivator MC 1000-OD (Photon System Instruments; Drásov, Czech Republic). Starter cultures (20 mL) were inoculated from plates and grown in liquid cultures as described above. Initial 70 mL cultures were inoculated at 0.3 OD_{730} in BGH11 and supplemented with 100 µg/mL kanamycin and

spectinomycin. Cultures were flushed with 3% CO_2 (*v*/*v*), grown at 30 °C, and in 100 µE of light. Samples were taken every 24 h for 7 day. Kanamycin (100 µg/mL) was supplemented each day. Cultures were induced on day 2 with 1 mM IPTG. Cells were harvested at the end of the run for further analysis.

2.3. Overlay Experiment

Overlay experiments were performed in 40 mL cultures in Erlenmeyer flasks in BGH11 supplemented with 50 mM $NaHCO_3$ and Na_2CO_3 with or without the addition of 10 mL *N*-dodecane. Flasks were grown at 30 °C with constant shaking under 100 µE of light. Initial cultures were inoculated at 0.2 OD_{730} and time points were taken every 24 h for 7 day. Cells and the overlay were harvested and stored in glass vials with PTFE lids for quantification of 13-R-MO using GC-MS analysis (Shimadzu, Ballerup, Denmark).

2.4. Cloning and Transformation

*Pb*TPS2, *Pb*TPS3, *Sj*GGDPS, *Pb*GGDPS, and *Sc*GGDPS were codon optimized and obtained from GenScript. All amplifications were performed using Q5 Polymerase (New England BioLabs; Ipswich, MA, USA). All cloning was performed using HiFi DNA Assembly (New England BioLabs). The TPS construct comprised of *Pb*TPS2 and *Pb*TPS3 in an operon driven by the Pcpc560 promoter and integrated into the pSL2387 backbone containing the NSP1 flanking homology regions. *Pb*TPS2 and *Pb*TPS3 were tagged with the Strep-II and HA tag respectively. The three GGDPSs were tagged with the HA tag and were driven by the *trc* promoter located on the pDF-trc backbone. Additionally, the *Sj*GG/D construct comprised of the *Sj*GGDPS and a mutant DXS in an operon [26]. The mutant DXS was generated by overlap extension PCR. All construct sequences used can be found in Supplementary Table S1.

Transformation was performed by either natural transformation for the integrative TPS construct or triparental mating for the replicative GGDPS constructs. Natural transformation was performed as follows. Roughly 10 mL of WT at an OD_{730} around 0.8 were spun down and washed once to remove any residual antibiotics. Cells were resuspended in 10 mL BGH11 and 200 µL of the resulting cell suspension were used per construct. Roughly 5 µg of purified plasmid was mixed with 200 µL of cells and incubated for 4 h at RT in 100 µE light. Cells were then plated on BGH5 plates without antibiotics and incubated for 1 day at 30 °C under 30 µE of light. After incubation for a day, the cells were scraped off the BGH5 plates and plated onto BGH5 plates with 25 µg/mL kanamycin. Following the appearance of single colonies, colonies were picked and restreaked onto BGH5 with 50 µg/mL kanamycin. This process was repeated until the strain was fully segregated. Triparental mating was performed as described in [27].

2.5. Western Blotting

Cell pellets on day 7 of the photobioreactor run were harvested from 10 mL of culture and resuspended in approximately 600 µL of 50 mM Tris-HCl pH 7.5 containing 2X cOmplete EDTA- free protease inhibitor (Roche; Copenhagen, Denmark). Zirconium oxide beads (200 µL, 0.15 mm diameter) were added to the cell suspension and disrupted using a NextAdvance Bullet Blender (Troy, NY, USA). Samples were processed 3 times at power 12 for 5 min each time. The resulting whole-cell lysate was quantified for total protein content using a Pierce BCA Protein Assay Kit (Thermo Scientific; Roskilde, Denmark).

Total protein (10 or 40 µg) was boiled at 90 °C for 5 min in 2% SDS/0.1 M DTT/10% glycerol/0.05 M Tris HCl pH 6.8 and applied onto 12% TGX stain-free gels (Bio-Rad; Copenhagen, Denmark). Gels were run at 250 V for 30–35 min in Tris-glycine-SDS buffer (Bio-Rad). Proteins were transferred onto a Trans-Blot Turbo PVDF membrane for 7 min at 2.5 A using a Trans-Blot Turbo blotting system (Bio-Rad). Membranes were blocked for 1 h at room temperature in 5% skim milk in PBS-T (PBS with 0.05% Tween-20) and washed with PBS-T. Primary anti-HA antibodies (dilution 1:1000) were applied for 1 h at room temperature in 2% skim milk in PBS-T with a. Membranes were washed in PBS-T and secondary swine anti-rabbit HRP conjugated antibodies (Dako; Glostrup, Denmark) (dilution of 1:5000) were applied in 2% skim milk in PBS-T with a for 1 h. Chemiluminescence was detected using Super Signal West Dura substrate (Thermo Scientific) using a ChemiDoc MP imaging system equipped with a cold CCD camera (Bio-Rad).

2.6. GC-MS Analysis

13-R-MO quantification was carried out using the cell pellet obtained from 10 to 20 mL of a day 7 culture from from the photobioreactor run. The pellet was resuspended in 8 mL of 10% methanolic KOH and the samples were

incubated at 65 °C for 1 h. Liquid-liquid extraction was performed by the addition of 2 mL of hexane. For quantification of 13-R-MO in the overlay, direct injection of dodecane from the overlay experiments was used.

GC-MS analysis was performed on a Shimadzu GCMS-QP2010 PLUS instrument using a HP-5MS UI column (20 m × 0.18 mm i.d.; 0.18 µm film thickness) (Shimadzu, Ballerup, Denmark). Sampling temperature and time occurred at 250 °C and 1 min in splitless mode. Chromatography was carried out using H_2 as the carrier gas, with a linear velocity of 50 cm/s, and a purge flow of 1 mL/min. The gradient used was as follows: 60 °C for 1 min; 60 °C increasing at a rate of 30 °C/min until reaching 150 °C; 150 °C increasing at a rate of 15 °C/min until reaching 250 °C; 250 °C increasing at a rate of 30 °C/min reaching 280 °C; hold at 280 °C for 3 min. 1 µL of either hexane or dodecane extract was injected into the column. The ion source temperature was set to 250 °C, with spectral recording between 50 *m*/*z* to 400 *m*/*z*. MS acquisition was set to start after 3 min or 8 min for hexane or dodecane extracts respectively.

3. Results

3.1. Strain Design and Construction

A base strain capable of producing 13-R MO was constructed by the introduction of the two terpene synthases, *Pb*TPS2 and *Pb*TPS3, from *Plectranthus barbatus* [7] (Figure 1A). The TPS cassette was introduced into the NSP1 neutral site under the control of the Pcpc560 promoter [28,29]. Two steps in the MEP pathway were chosen for engineering in accordance with the "push-pull" strategy, namely DXS and GGDPS. DXS is positioned at the start of the MEP pathway and catalyzes the condensation of two central carbon metabolites, glyceraldehyde-3-phosphate and pyruvate. GGDPS catalyzes the condensation of 4 units of DMADP and IDP in order to form geranylgeranyl diphosphate, the substrate of *Pb*TPS2 and *Pb*TPS3 [11]. A prokaryotic, a yeast, and a plant derived GGDPS was selected for screening: *Synechococcus* JA-3-3Ab (*Sj*GGDPS), *Plectranthus barbatus* (*Pb*GGDPS), and *Saccharomyces cerevisiae* (*Sc*GGDPS). *Sj*GGDPS was chosen among cyanobacterial GGDPS to represent a prokaryotic enzyme and was previously used to enhance forskolin titers in yeast [30]. *Pb*GGDPS was chosen as derived from the original host organism of the forskolin biosynthetic pathway. Enzymes from the same biosynthetic pathway are known to be able to form protein-protein interactions that can potentially facilitate substrate channeling [31–34]. *Sc*GGDPS was chosen due to its evolutionary divergence from both plants and cyanobacteria, potentially avoiding endogenous feedback regulation that may or may not occur in *Synechocystis*. An alignment of all three GGDPSs is shown in Figure S1, where *Sc*GGDPS is shown to differ drastically from both *Sj*GGDPS and *Pb*GGDPS by the presence of two extra sequences inserted at the C-terminus. Mutations from a DXS variant shown to be responsible for the high monoterpenol content in a *Vitis vinifera* cultivar were introduced into *E. coli* DXS and expressed in an operon with the cyanobacterial *Sj*GGDPS (resulting in *Sj*GG/D) [26]. All resulting constructs were introduced into the replicative pDF-trc under the IPTG inducible Ptrc promoter.

3.2. Growth Characterization and Expression

Initial verification of transformants and their possible ability to produce 13-R-MO was carried out by culturing transformants in a photobioreactor for 7 day. Strains were grown in triplicate as described in the Materials and Methods. No large or significant effect on the final cell density between any of the strains was observed (Figure 1B). One particular transformant carrying the *Sj*GG/D construct grew slower and reached a lower final OD_{730} than the other two strains carrying the same construct. The growth of transformant *Sj*GG/D T3 is shown in Figure 1B (light blue diamonds). The final OD_{730} of the other two transformants were 5.0 and 5.2, while the final OD_{730} of *Sj*GG/D T3 only reached 3.9. This transformant was later found to be the sole transformant from the *Sj*GG/D construct capable of producing 13-R-MO.

Cells were harvested after 7-day of growth and were analyzed for protein expression. *Pb*TPS3 and all three GGDPSs were tagged with HA. The expected sizes for *Pb*TPS3, *Sj*GGDPS, *Pb*GGDPS, and *Sc*GGDPS are 68.7, 33.0, 32.6, and 39.7 kDa, respectively. *Pb*TPS2 was tagged with strepII but was not monitored as the antibody did not bind well, while DXS was untagged. Normalization was done by equal loading (10 µg total protein content). All strains expressed the expected proteins. Except for *Sj*GG/D T1 and T2 (Figure 1C), appearance of minor potential degradation products was also observed. All *Sj*GG/D strains were re-run with 40 µg of total protein content to confirm if the absence of the expected bands was due to low expression (Figure 1D). Strains *Sj*GG/D T1 and T2 did not express *Pb*TPS3 or *Sj*GGDPS In Figure S2, PCR genotyping shows the presence of the *Sj*GGDPS and *Ec*DXS gene construct in all three

*Sj*GG/D transformants (T1-T3), suggesting suppression of expression due to metabolic stress. This correlates with the differences in growth seen in the *Sj*GG/D transformants (Figure 1B).

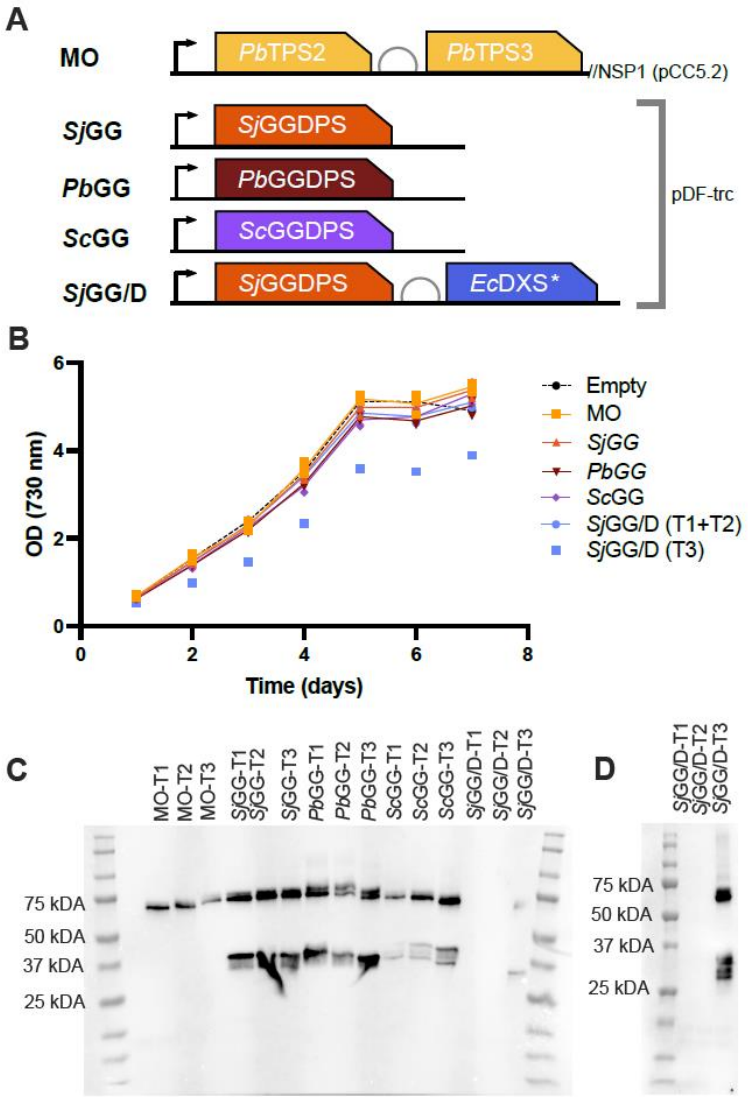

Figure 1. Constructed strains and initial characterization of transformants. (**A**) The base strain MO was constructed by integration of *Pb*TPS2 and *Pb*TPS3 under the strong Pcpc560 promoter into the NSP1 neutral site. Additional strains were constructed by transforming the base strain with the replicative plasmid pDF-trc containing the *Synechococcus* sp. JA-3-3Ab GGDPS (*Sj*GG), the *Plectranthus barbatus* GGDPS (*Pb*GG), the *Saccharomyces cerevisiae* GGDPS (*Sc*GG), and the *Synechococcus* sp. JA-3-3Ab GGDPS with an *E. coli* DXS mutant (*Sj*GG/D). (**B**) OD_{730} measurements of strains grown in a photobioreactor. All strains except the empty control strain (n = 1) were grown in triplicate. T1-T3 indicates three independent transformants. *Sj*GG/D transformant 3 (T3) was plotted separately, due to its marked deviation from the other two transformants (T1 + T2). One-way ANOVA of day 7 OD_{730} values showed no significance. (**C**) Western blot showing the expression of the HA tagged GGDPSs as well as the HA-tagged *Pb*TPS3. Lanes were normalized by loading 10 µg total protein. (**D**) Anti-HA Western blot of the *Sj*GG/D transformants (T1–T3) with 40 µg total protein loaded per lane.

3.3. 13-R-manoyl Oxide Titers after 7 Days

Cells collected from day 7 of the photobioreactor run were extracted and 13-R-MO was quantified by GC-MS (Figure 2). The base strains (MO), containing *Pb*TPS2 and *Pb*TPS3, showed the lowest production of 13-R-MO (Figure 3A). All other strains, containing GGDPS', had at least one replicate with greater than 4-fold increase over the average base strain titer. Fold increases ranged from 4.6 to 5.5-fold for *Sj*GG, from 1-fold to 4.2-fold for *Pb*GG, from 1.6 to 14-fold for *Sc*GG, and 11.6fold for the only *Sj*GG/D transformant (T3) capable of 13-R-MO production. The highest titers measured was in a *Sc*GG replicate at 11.8 mg/L, with the second highest measured at 9.7 mg/L in the *Sj*GG/D T3 replicate. As seen in Figure 1C, strains carrying the *Pb*GG and *Sc*GG construct showed a greater variance in protein expression in comparison with the cyanobacterial GGDPS in strain *Sj*GG. The *Sj*GGDPS was therefore used in

combination with *Ec*DXS to create the *Sj*GG/D strain. The highest titers shift to the *Sj*GG/D transformant 3 (T3) was grown in triplicate (Figure 3B).

Due to the toxicity of GGDP, overexpression of a GGDPS in yeast has been reported to result in the secretion of geranylgeraniol or geranyllinalool as detoxification products [35]. Geranyllinalool is formed by the spontaneous isomerization of geranylgeraniol in an acidic environment. We therefore investigated whether excess flux was directed towards side products. Analysis of 10 mL of supernatant did not detect any geranylgeraniol or geranyllinalool secreted to the media (Figure S3). The single constituent in the chromatograms is the internal standard 1-eicosene.

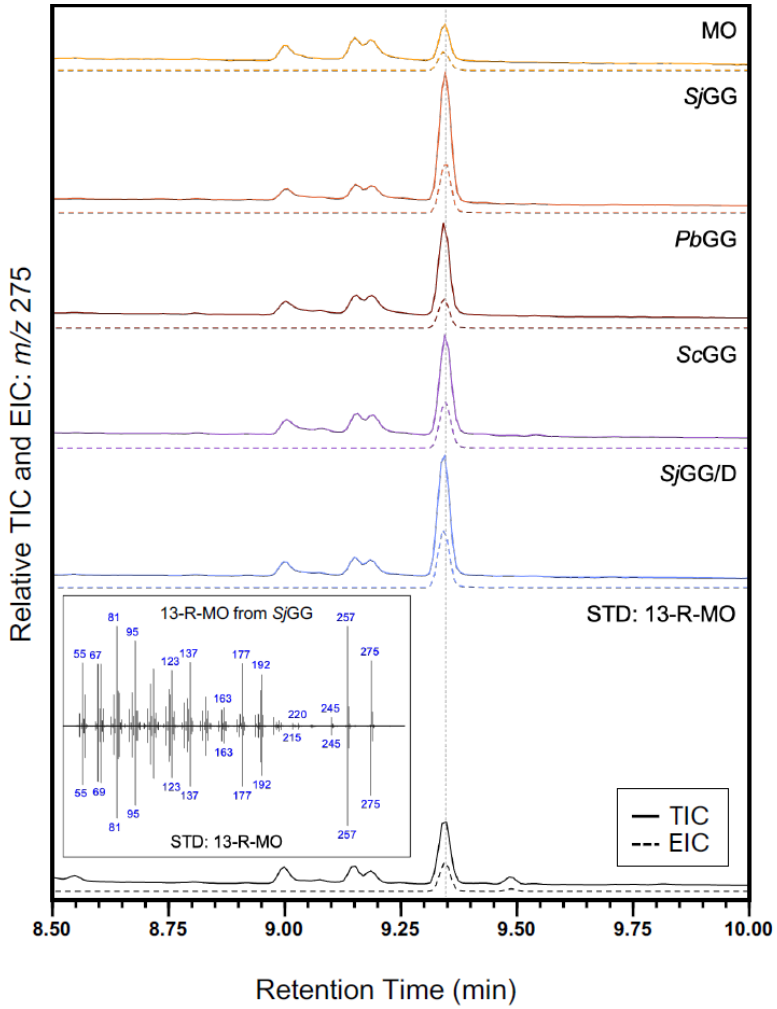

Figure 2. Detection of 13-MO by GC–MS analysis. Cell extracts were used to measure 13-R-MO of each engineered strain used in this study by GC-MS and verified using an authentic 13-R-MO standard (bottom). Both the relative total ion chromatograms (TIC) and the extracted ion chromatograms (EIC) at *m/z* 275 are plotted for each strain and the standard. The mass spectra of the main peaks at around 9.35 min for both *Sj*GG and the standard are also plotted to confirm the correct identical fragmentation patterns.

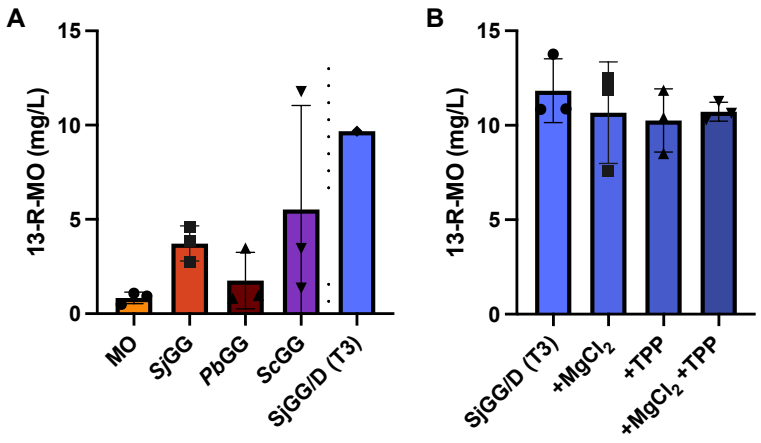

Figure 3. 13-R-MO titers from a 7 d photobioreactor experiment. (**A**) Three transformants of each construct were grown in the photobioreactor and 13-R-MO was quantified on the 7th day. Since *Pb*TPS3 or *Sj*GGDPS was not expressed in *Sj*GG/D T1 and T2, they were excluded from the figure. (**B**) 13-R-MO titers for *Sj*GG/D (T3), grown in triplicate, supplemented with 400 mM $MgCl_2$, 150 mM TPP, or both. There is no significant difference in production between groups (one-way ANOVA). The titers normalized to OD730 is shown in Figure S4A,B.

3.4. Enzyme Co-factors Are Not Limiting

Both *Pb*TPSs and *Ec*DXS* are dependent on the presence of co-factors to be catalytically active. TPS coordinates Mg^{2+} ions while DXS coordinates Mg^{2+} and thiamine pyrophosphate (TPP). In *Synechococcus elongatus* 7942, production of ethanol was improved by increasing the concentration of essential co-factors in the media [36]. Accordingly, we supplemented the growth medium for the *Sj*GG/D (T3) strain with 400 mM $MgCl_2$, 150 mM TPP, or both. Each experimental condition was carried out in triplicate and the resulting 13-R-MO titers were measured (Figure 3B). No significant differences were detected between the conditions tested and cofactors are therefore not the limiting factor.

3.5. Adding an Organic Overlay Increases the Production of 13-R-manoyl Oxide

Because 13-R-MO was discovered not to be excreted to the media in any significant amount, the possibility of increasing the production of 13-R-MO by orchestrating an artificial sink for 13-R-MO was examined. In this experimental setup, 40 mL cultures were grown in flasks with and without a 10 mL *N*-dodecane overlay. A minor growth inhibition in all strains was observed between the standard and overlay conditions including the "Empty" control strain (Figure 4B). The introduction of an overlay increased 13-R-MO titers in all conditions (Figure 4A) by a factor of 2.6 except for the *Sj*GG/D strain, where no meaningful increase was observed. Cultures without overlay exclusively were found to have 13-R-MO in the cell fraction. Cultures with overlay were quantified solely with the overlay fraction due to negligible amounts in the cell fraction (below quantification limit). When the data are normalized to OD_{730} to account for the effects of overlay growth inhibition, normalized titers showed an increase of a factor of 4 for all GGDPS only constructs and an increase of a factor of 9.8 for the the *Sj*GG/D construct (Figure S4C).

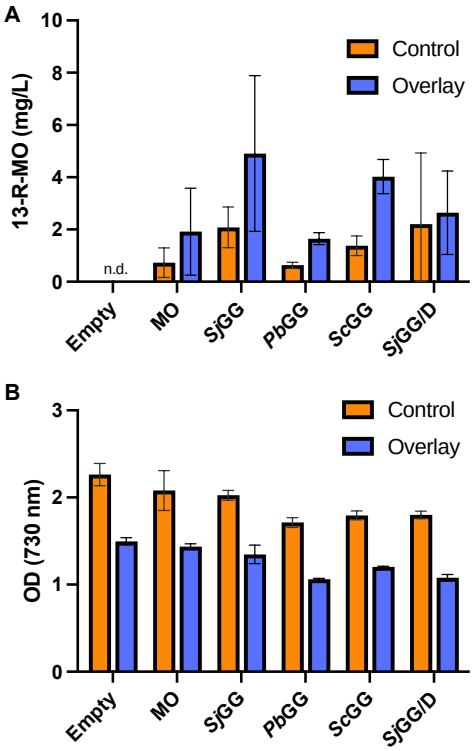

Figure 4. Shake flask experiment with *n*-dodecane overlays. **(A)** Day 7 13-R-MO titers of each culture with and without (i.e. control) *N*-dodecane overlays. (**B**) 7-day end point OD_{730} measurements of strains cultured with and without an *N*-dodecane overlay.

4. Discussion

The carbon flux through the MEP pathway in the cyanobacterium *Synechocystis* PCC. 6803 was enhanced by expression of *Ec*DXS* and *Sj*GGDPS. Co-expression of the two diterpenoid synthases *Pb*TPS2 and *Pb*TPS3 from *P. barbatus* with *Ec*DXS* and *Sj*GGDPS resulted in the production of the diterpenoid 13-R-manoyl oxide at a titer of 9.7 mg/L, an 11-fold increase in titer compared to expression in the base strain. Removal of 13-R-MO from the culture medium by introduction of an *n*-dodecane overlay increased titers on average 2.6 fold in a separate cultivation system.

4.1. Overexpression of Both DXS and GGDPS Shows Growth Defects

During the course of a 7-day photobioreactor experiment, GGDPS over-expression strains showed no significant growth inhibition compared with the control strain. The single transformant that produced 13-R-MO with the *Sj*GG/D construct grew much slower compared to the WT (Figure 1B). It is unlikely that this growth defect is due to altered partitioning of central carbon metabolites to produce 13-R-MO as the resulting 13-R-MO yield was low compared to the carbon equivalents needed to make up for the difference in growth. Instead, toxicity from the 13-R-MO produced may play a role since it is not excreted and thus stored within the cells. Due to its hydrophobic nature, it is plausible that the 13-R-MO produced might partition into the *Synechocystis* membranes or form droplets and thus perturb the membrane function/fluidity. A previous study on a squalene-producing strain of *Synechococcus elongatus* PCC 7942 demonstrated squalene droplets forming between distorted thylakoid membranes coupled with a measurable growth defect [37]. There was also noticeable variation in the protein expression seen by the western blot for *Sc*GGDPs. While this difference in expression cannot be explained for certain, it could be due to the toxic effects of 13-R-MO.

4.2. Pathway Manipulation and Overlays Increase Titers

The use of an overlay resulted in a 2.6 fold increase in titers when compared to cultures without overlays. The results indicate that removal of 13-R-MO from the cells potentially causes favorable shifts in the reaction equilibrium and/or relieves stress caused by 13-R-MO which in turn increases total amounts of 13-R-MO produced. Our results also show that the use of *n*-dodecane as an overlay inhibited growth, however the growth inhibition was not enough to negate the increased production driven by product removal. A previous study demonstrated slight *N*-dodecane toxicity when used as an overlay for the sequestration of squalene and amorphadiene [38]. However, the use of hexadecane and

tetradecane did not result in growth defects. Comparing the normalized titers between the photobioreactor and flask runs shows that in general the normalized titers in the flasks were much lower (Figure S4C). The source of this discrepancy is likely due to the different culturing conditions, particularly the absence of CO_2 supplementation when grown in flasks. This could suggest that the CO_2 supply is a limiting factor for the production of 13-R-MO. Furthermore, the *Sj*GG/D was no longer superior to the other constructs under the flask conditions when compared to the photobioreactor conditions.

4.3. Attemted Optimization of 13-R-MO Production

As demonstrated by Velmurugan and Incharoensakdi [36], the enzymes expressed in this study also use Mg^{2+} and TPP as co-factors, but the supplementation of these co-factors did not result in an increase in production. One major difference between our study and Velmurugan and Incharoensakdi [36] was the length of the culture period and it is possible that if we had extended our culture length, benefits of supplementation of co-factors would have become apparent. Another explanation could be that a portion of our overexpressed enzymes were not properly folded and thus would not benefit from the increased supply of co-factors. DXS is of particular concern as it is known to be prone to aggregation in chloroplasts and needs reactivation to gain activity [39]. It is unclear whether these pathways are present in cyanobacteria, although homologs can be found. Activation of the refolding pathway could potentially further increase flux through the MEP pathway.

Production of 13-R-MO was also introduced into the model photosynthetic eukaryote green algae *Chlamydomonas reinhardtii* resulting in 50 mg/L of 13-R-MO [40]. The authors used a GGDPS-antibiotic resistance gene-*Pb*TPS2 fusion construct in a 16:8 light/dark growth cycle with a *N*-dodecane overlay in order to achieve these titers. Fusion of the terpene synthase with the GGDPS along with the use of a different light regime should be implemented in *Synechocystis* in order to see if any further improvements can be made as shown in *C. reinhardtii*. A cultivation strategy with a 16:8 light/dark growth cycle was tested with the *Synechocystis* strains generated in the current study but it did not improve production (data not shown).

4.4. Perspectives

Manoyl Oxide (13-R-MO) formation is the first committed step in forskolin biosynthesis. This is followed by five oxygenation events on the carbon skeleton catalyzed by three P450s and finally an acetyltransferase completes the biosynthesis of forskolin [8]. Thus, in future experiments, the MO boosting presented here should be combined with the three P450s and the acetyltransferase. In this context, the P450 enzymes require reducing equivalents such as ferredoxin or NADPH to complete their catalytic cycle. Both reducing equivalents are generated through photosynthesis, making the forskolin pathway an ideal target for heterologous production in cyanobacteria. Previous studies have demonstrated the transfer of electrons from photosystem I (PSI) to cytochrome P450s using endogenous soluble electron donors, eliminating the need for a dedicated reductase [41–46]. Among the two photosystems embedded in the thylakoid membranes, PSI stands out as the most stable. Even when subjected to photoinhibitory conditions, it is shielded by alterations in cyclic electron transport around PSI [47]. Consequently, the light-driven synthesis reliant on electron donation from PSI exhibits remarkable robustness.

Supplementary Materials

The following supporting information can be found at: https://www.sciepublish.com/article/pii/151.

Acknowledgments

We would like to thank Himadri Pakrasi for the plasmid pSL2387.

Author Contributions

L.C.S., P.E.J. and T.G. designed the experiments. L.C.S., N.D., S.L.W., and N.J.B. performed the experiments. L.C.S. analyzed the data and wrote a draft manuscript. L.C.S., P.E.J., N.D., and B.L.M. wrote the final manuscript.

Ethics Statement

Not applicable.

Informed Consent Statement

Not applicable.

Funding

The authors acknowledge financial support from: (1) Center for Synthetic Biology "bioSYNergy" (UCPH Excellence Program for Interdisciplinary Research), (2) Innovation Fund Denmark (Project no: 12-131834), (3) Novo Nordisk Foundation (NNF13OC0005685; NNF19OC0057634; NNF19OC0054563), (4) VILLUM Foundation (Project no: 13363), (5) VILLUM Center for Plant Plasticity (Project No. VKR023054) and (6) European Research Council Advanced Grant (ERC-2012-ADG_20120314, Project no: 323034).

Declaration of Competing Interest

The authors do not declare any conflicts of interest.

References

1. Nielsen AZ, Mellor SB, Vavitsas K, Wlodarczyk AJ, Gnanasekaran T, Ramos H de Jesus MP, et al. Extending the biosynthetic repertoires of cyanobacteria and chloroplasts. *Plant J.* **2016**, *87*, 87–102.
2. Lassen LM, Zygadlo Nielsen A, Friis Ziersen BE; Gnanasekaran T, Møller BL, Jensen PE. Redirecting photosynthetic electron flow into light-driven synthesis of alternative products including high-value bioactive natural compounds. *ACS Synth. Biol.* **2014**, *3*, 1–12.
3. Sørensen M, Andersen-Ranberg J, Hankamer B, Møller BL. Feature Article: Circular biomanufacturing through harvesting solar energy and CO_2. *Trends Plant Sci.* **2022**, *27*, 655–673.
4. Pichersky E, Raguso RA. Why do plants produce so many terpenoid compounds? *New. Phytol.* **2018**, *220*, 692–702.
5. Cheng AX, Lou YG, Mao YB, Lu S, Wang LJ, Chen XY. Plant terpenoids: biosynthesis and ecological functions. *J. Integr. Plant Biol.* **2007**, *49*, 179–186.
6. Moser S, Pichler H. Identifying and engineering the ideal microbial terpenoid production host. *Appl. Microbiol. Biotechnol.* **2019**, *103*, 5501–5516.
7. Pateraki I, Andersen-Ranberg J, Hamberger Britta, Heskes AM, Martens HJ, Zerbe P, et al. Manoyl oxide (13R), the biosynthetic precursor of forskolin, is synthesized in specialized root cork cells in Coleus forskohlii. *Plant Physiol.* **2014**, *164*, 1222–1236.
8. Pateraki I, Andersen-Ranberg J, Jensen NB, Wubshet SG, Heskes AM, Forman V, et al. Total biosynthesis of the cyclic AMP booster forskolin from Coleus forskohlii. *eLife* **2017**, *6*, e23001.
9. Forman V, Luo D, Lemcke R, Nelson DR. Staerk D, Kampranis S, et al. A gene cluster in Ginkgo biloba encoding for unique multifunctional cytochrome P450s orchestrates key steps in ginkgolide biosynthesis. *Nat. Commun.* **2022**, *13*, 5143.
10. Hansen NL, Kjærulff L, Heck Q, Forman V, Stærk D, Møller BL, et al. Tripterygium wilfordii cytochrome P450s catalyze the key methyl shift and epoxidations in biosynthesis of triptonide. *Nat. Commun.* **2022**, *13*, 5011.
11. Pattanaik B, Lindberg P. Terpenoids and their biosynthesis in cyanobacteria. *Life* **2015**, *5*, 269–293.
12. Bathe U, Tissier A. Cytochrome P450 enzymes: A driving force of plant diterpene diversity. Phytochemistry **2019**, *161*, 149–162.
13. Gericke O, Hansen NL, Pedersen GB, Kjaerulff L, Luo D, Staerk D, et al. Nerylneryl diphosphate is the precursor of serrulatane, viscidane and cembrane-type diterpenoids in Eremophila species. *BMC Plant Biol.* **2020**, *20*, 91.
14. Luo D, Callari R, Hamberger B, Wubshet SG, Nielsen MT, Andersen-Ranberg J, et al. Oxidation and cyclization of casbene in the biosynthesis of Euphorbia factors from mature seeds of Euphorbia lathyris L. *Proc. Natl. Acad. Sci. USA* **2016**, *113*, E5082–E5089.
15. Mills LA, McCormick AJ, Lea-Smith DJ. Current knowledge and recent advances in understanding metabolism of the model cyanobacterium Synechocystis sp. PCC 6803. *Biosci. Rep.* **2020**, *40*, BSR20193325.
16. Rodrigues JS, Lindberg P. Engineering cyanobacteria as host organisms for production of terpenes and terpenoids. In *Cyanobacteria Biotechnology*; Nielsen J, Lee S, Stephanopoulos G, Hudson P, Eds; Wiley: Hoboken, NJ, USA, 2021; pp. 267–300.
17. Leonard E, Ajikumar PK, Thayer K, Xiao W-H, Mo JD, Tidor B, et al. Combining metabolic and protein engineering of a terpenoid biosynthetic pathway for overproduction and selectivity control. *Proc. Natl. Acad. Sci. USA* **2010**, *107*, 13654–13659.

18. Tian, S, Wang D, Yang L, Zhang, Z, Liu, L. A systematic review of 1-Deoxy-D-xylulose-5-phosphate synthase in terpenoid biosynthesis in plants. *Plant Growth Regul.* **2022**, *96*, 221–235.
19. Volke DC, Rohwer J, Fischer R, Jennewein S. Investigation of the methylerythritol 4-phosphate pathway for microbial terpenoid production through metabolic control analysis. *Microb. Cell Fact*. **2019**, *18*, 192.
20. Klaus O, Hilgers F, Nakielski A, Hasenklever D, Jaeger K-E, Axmann IM, et al. Engineering phototrophic bacteria for the production of terpenoids. *Curr. Opin. Biotechnol.* **2022**, *77*, 102764.
21. Ajikumar PK, Xiao W-H, Tyo KEJ, Wang Y, Simeon F, Leonard E, et al. Isoprenoid Pathway Optimization for Taxol Precursor Overproduction in *Escherichia coli*. *Science* **2010**, *330*, 70–74.
22. Brückner K, Tissier A. High-level diterpene production by transient expression in Nicotiana benthamiana. *Plant Methods* **2013**, *9*, 46.
23. Englund E, Andersen-Ranberg J, Miao R, Hamberger B, Lindberg P. Metabolic Engineering of Synechocystis sp. PCC 6803 for Production of the Plant Diterpenoid Manoyl Oxide. *ACS Synth. Biol.* **2015**, *4*, 1270–1278.
24. Guerrero F, Carbonell V, Cossu M, Correddu D, Jones PR. Ethylene Synthesis and Regulated Expression of Recombinant Protein in Synechocystis sp. PCC 6803. *PLoS ONE* **2012**, *7*, e50470.
25. Stanier RY, Kunisawa R, Mandel M, Cohen-Bazire G. Purification and properties of unicellular blue-green algae (order Chroococcales). *Bacteriol. Rev.* **1971**, *35*, 171–205.
26. Hugueney P, Duchene E, Merdinoglu D. 1-deoxy-D-xylulose 5-phosphate synthase alleles responsible for enhanced terpene biosynthesis. DK2630157T3, 2012.
27. Casella S, Huang F, Mason D, Zhao G-Y, Johnson GN, Mullineaux CW, et al. Dissecting the Native Architecture and Dynamics of Cyanobacterial Photosynthetic Machinery. *Mol. Plant* **2017**, *10*, 1434–1448.
28. Ng AH, Berla BM, Pakrasi HB. Fine-tuning of photoautotrophic protein production by combining promoters and neutral sites in the cyanobacterium Synechocystis sp. strain PCC 6803. *Appl. Environ. Microbiol.* **2015**, *81*, 6857–6863.
29. Zhou J, Zhang H, Meng H, Zhu Y, Bao G, Zhang Y, et al. Discovery of a super-strong promoter enables efficient production of heterologous proteins in cyanobacteria. *Sci. Rep.* **2014**, *4*, 1–6.
30. Forman V, Bjerg-Jensen N, Dyekjær JD, Møller BL, Pateraki I. Engineering of CYP76AH15 can improve activity and specificity towards forskolin biosynthesis in yeast. *Microb. Cell Fact.* **2018**, *17*, 181.
31. Møller BL, Conn EE. The biosynthesis of cyanogenic glucosides in higher plants. Channeling of intermediates in dhurrin biosynthesis by a microsomal system from Sorghum bicolor (Linn.) Moench. *J. Biol. Chem.* **1980**, *255*, 3049–3056.
32. Laursen T, Borch J, Knudsen C, Bavishi K, Torta F, Martens HJ, et al. Characterization of a dynamic metabolon producing the defense compound dhurrin in sorghum. *Science* **2016**, *354*, 890–893
33. Jørgensen K, Rasmussen AV, Morant M, Nielsen AH, Bjarnholt N, Zagrobelny M, et al. Metabolon formation and metabolic channeling in the biosynthesis of plant natural products. *Curr. Opin. Plant Biol.* **2005**, *8*, 280–291.
34. Zhou F, Wang CY, Gutensohn M, Jiang L, Zhang P, Zhang D, et al. A recruiting protein of geranylgeranyl diphosphate synthase controls metabolic flux toward chlorophyll biosynthesis in rice. *Proc. Natl. Acad. Sci. USA* **2017**, *114*, 6866–6871.
35. Ignea C, Trikka FA, Nikolaidis AK, Georgantea P, Ioannou E, Loupassaki S, et al. Efficient diterpene production in yeast by engineering Erg20p into a geranylgeranyl diphosphate synthase. *Metab. Eng.* **2015**, *27*, 65–75.
36. Velmurugan R, Incharoensakdi A. Heterologous Expression of Ethanol Synthesis Pathway in Glycogen Deficient Synechococcus elongatus PCC 7942 Resulted in Enhanced Production of Ethanol and Exopolysaccharides. *Front. Plant Sci.* **2020**, *11*, 74.
37. Choi SY, Sim SJ, Choi JI, Woo HM. Identification of small droplets of photosynthetic squalene in engineered Synechococcus elongatus PCC 7942 using TEM and selective fluorescent Nile red analysis. *Lett. Appl. Microbiol.* **2018**, *66*, 523–529.
38. Choi SY, Lee HJ, Choi J, Kim J, Sim SJ, Um Y, et al. Photosynthetic conversion of CO2 to farnesyl diphosphate-derived phytochemicals (amorpha-4,11-diene and squalene) by engineered cyanobacteria. *Biotechnol. Biofuels* **2016**, *9*, 202.
39. Pulido P, Llamas E, Llorente B, Ventura S, Wright LP, Rodríguez-Concepción M. Specific Hsp100 Chaperones Determine the Fate of the First Enzyme of the Plastidial Isoprenoid Pathway for Either Refolding or Degradation by the Stromal Clp Protease in Arabidopsis. *PLoS Genet.* **2016**, *12*, e1005824.
40. Lauersen KJ, Wichmann J, Baier T, Kampranis SC, Pateraki I, Møller BL, et al. Phototrophic production of heterologous diterpenoids and a hydroxy-functionalized derivative from Chlamydomonas reinhardtii. *Metab. Eng.* **2018**, *49*, 116–127.
41. Mellor SB, Vinde MH, Nielsen AZ, Hanke GT, Abdiaziz K, Roessler MM, et al. Defining optimal electron transfer partners for light-driven cytochrome P450 reactions. *Metab. Eng.* **2019**, *55*, 33–43.
42. Nielsen AZ, Ziersen B, Jensen K, Lassen LM, Olsen CE, Møller BL, et al. Redirecting Photosynthetic Reducing Power toward Bioactive Natural Product Synthesis. *ACS Synth. Biol.* **2013**, *2*, 308–315.

43. Wlodarczyk A, Gnanasekaran T, Nielsen AZ, Zulu NN, Mellor SB, Luckner M, et al. Metabolic engineering of light-driven cytochrome P450 dependent pathways into *Synechocystis* sp. PCC 6803. *Metab. Eng.* **2016**, *33*, 1–11.
44. Berepiki A, Hitchcock A, Moore CM, Bibby TS. Tapping the unused potential of photosynthesis with a heterologous electron sink. *ACS Synth. Biol.* **2016**, *5*, 1369–1375.
45. Berepiki A, Gittins JR, Moore CM, Bibby TS. Rational engineering of photosynthetic electron flux enhances light-powered cytochrome P450 activity. *Synth. Biol.* **2018**, *3*, ysy009.
46. Santos-Merino M, Torrado A, Davis GA, Röttig A, Bibby TS, Kramer DM, et al. Improved photosynthetic capacity and photoprotection via heterologous metabolism engineering in cyanobacteria. *Proc. Natl. Acad. Sci. USA* **2020**, *118*, e2021523118.
47. Teicher HB, Møller BL, Scheller HV. Photoinhibition of Photosystem I in field-grown barley (Hordeum vulgare L.): Induction, recovery and acclimation. *Photosynth. Res.* **2000**, *64*, 53–61.